Mechanistic Insight into Gas-Phase Reactions of $H^{\cdot} + Si_2H_6$ and Hydrogen Atom Etching of Silicon Surfaces

Kerwin D. Dobbs*,† and Douglas J. Doren*,‡

Contribution from DuPont Central Research and Development, Experimental Station, P.O. Box 80328, Wilmington, Delaware 19880, and the Department of Chemistry, University of Delaware, Newark, Delaware 19716

Received September 2, 1992

Abstract: The mechanism for the reaction of a hydrogen atom with a silicon surface trihydride species was investigated by ab initio molecular orbital techniques. This reaction is believed to be the final step in the overall mechanism for the etching of silicon surfaces by hydrogen atoms. The gas-phase reaction of disilane with a hydrogen atom to form silyl radical and silane was used as the model for the etching process. Two transition-state structures exist for this exchange reaction: (1) backside attack of a silyl group by the hydrogen atom and (2) frontside attack of the SiSi bond by the hydrogen atom. Calculations show a lower activation energy for frontside attack (3.0 kcal mol^{-1}) than for backside attack (5.8 kcal mol^{-1}). Hydrogen abstraction is a strong competing reaction to frontside attack, having a calculated activation barrier of 2.4 kcal mol^{-1}. These model calculations reproduce what is known experimentally about the gas-phase reactions of hydrogen radicals with disilane and provide new insight regarding silicon surface etching by hydrogen atoms.

Reactions that involve hydrogen and silyl radicals are fundamental in plasma etching of silicon surfaces and plasma-assisted deposition of silicon. Exposing silicon surfaces to atomic hydrogen can result in etching, with silane or disilane as products.[1-4] As a potential application, this reaction may be used as an in situ source of silanes for chemical vapor deposition (CVD).[3] The reaction has also been exploited in Boland's suggestion that an STM may be used to explore subsurface layers of semiconductors after etching away the topmost layer with hydrogen.[5] Mechanisms proposed for etching all have reaction 1 as a final step,

$$\equiv\!\!\equiv Si\text{–}SiH_3 + H^{\cdot} \rightarrow \equiv\!\!\equiv Si\text{–} + SiH_4 \qquad (1)$$

where "$\equiv\!\!\equiv$" indicates three bonds from silicon to the surface and "–" indicates a Si dangling bond. The mechanistic details of this reaction are unclear; since hydrogen has both nucleophilic and electrophilic character, it may conceivably attack from either the backside of the silyl group or it may make a frontside attack on the SiSi bond. In ultrahigh vacuum conditions, with hydrogen adsorbed on the surface, a Langmuir–Hinshelwood reaction probably proceeds by frontside attack.[1] However, with a flux of H atoms, as from a molecular beam or plasma, backside attack by an Eley–Rideal mechanism may occur as well. Competition between these potential mechanisms can only be understood if we know the activation energy for each pathway.

The reverse of reaction 1 (reaction 2)is the dissociative

$$\equiv\!\!\equiv Si\text{–} + SiH_4 \rightarrow \equiv\!\!\equiv Si\text{–}SiH_3 + H^{\cdot} \qquad (2)$$

adsorption of silane at a dangling bond site. This reaction is the first step in CVD of silicon from silane.[6-9] Because the probability of this reaction under thermal conditions is so low ($\sim 10^{-5}$), it is difficult to study experimentally,[7] and silicon film growth from silane is typically enhanced by plasma or photochemical CVD conditions.

Gas-phase reactions analogous to (1) and (2) occur in silane plasmas. In reactions 3 and 4, silicon atoms have bonds to

$$H_3Si\text{–}SiH_3 + H^{\cdot} \rightarrow H_3Si^{\cdot} + SiH_4 \qquad (3)$$

$$H_3Si^{\cdot} + SiH_4 \rightarrow H_3Si\text{–}SiH_3 + H^{\cdot} \qquad (4)$$

hydrogen rather than bonds to the surface, as in (1) and (2). Robertson and Gallagher[10] have shown that $H^{\cdot}$ and $H_3Si^{\cdot}$ radicals are the dominant species reaching the surface in plasma CVD. The rate of reaction 3 has been determined by flash photolysis.[11] Reaction 4 is thermodynamically unfavorable, but Loh and Jasinski[12] have determined an upper bound to the rate.

In plasma deposition conditions, dangling bonds on the silicon surface are saturated by hydrogen. The dominant silicon species deposited is the $H_3Si^{\cdot}$ radical,[10] which can displace a hydrogen atom in a reaction similar to (4):

$$H_3Si^{\cdot} + \equiv\!\!\equiv Si\text{–}H \rightarrow \equiv\!\!\equiv Si\text{–}SiH_3 + H^{\cdot} \qquad (5)$$

These reactions represent a small part of the network of reactions that occur in the gas phase and at the surface under a variety of materials processing conditions. They are all closely related; if silicon bonds to the surface could be replaced by SiH bonds, reactions 1 and 3 and the reverse of reaction 5 would be identical. We have been interested in modeling reactions at semiconductor surfaces by using small silicon clusters to represent the surface. The smallest possible cluster consists of a single Si atom with bonds to the surface represented by three SiH bonds. The remaining Si bond can be empty to represent a surface dangling bond, or it may be bonded to an "adsorbate," such as H or SiH_3. Modeling the silicon surface in this simple way allows us to focus attention on a localized reaction, but it is obviously inadequate for many other surface reactions (specifically, any reaction that involves more than one surface site and reactions

† DuPont, Contribution No. 6337.
‡ University of Delaware.

(1) Gates, S. M.; Kunz, R. R.; Greenlief, C. M. *Surf. Sci.* **1989**, *207*, 364.
(2) Abrefah, J.; Olander, D. R. *Surf. Sci.* **1989**, *209*, 291.
(3) Sengupta, S. Ph.D. Dissertation, University of Delaware, Newark, DE, 1991.
(4) Lu, Z. H.; Griffiths, K.; Norton, P. R.; Sham, T. K. *Phys. Rev. Lett.* **1992**, *68*, 1343.
(5) Boland, J. *Science* **1992**, *255*, 186.
(6) Farnaam, M. K.; Olander, D. R. *Surf. Sci.* **1984**, *145*, 390.
(7) Gates, S. M.; Greenlief, C. M.; Beach, D. B.; Holbert, P. A. *J. Chem. Phys.* **1990**, *92*, 3144.
(8) Gates, S. M.; Kulkarni, S. K. *Appl. Phys. Lett.* **1991**, *58*, 2963.
(9) Jasinski, J. M.; Gates, S. M. *Acc. Chem. Res.* **1991**, *24*, 9.
(10) Robertson, R.; Gallagher, A. *J. Appl. Phys.* **1986**, *59*, 3402.
(11) Fabry, L.; Potzinger, P.; Reimann, B.; Ritter, A.; Steenbergen, H. P. *Organometallics* **1986**, *5*, 1231.
(12) Loh, S. K.; Jasinski, J. M. *J. Chem. Phys.* **1991**, *95*, 4914.

0002-7863/93/1515-3731$04.00/0

Scheme I

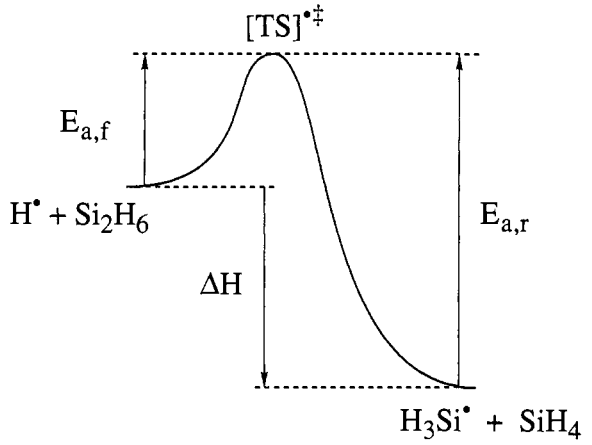

on reconstructed surfaces where silicon atoms are in a nontetrahedral environment). However, using a small Si cluster to model surface processes at single sites has proven highly successful for understanding surface etching by HF solutions[13] and vibrational energy transfer for H adsorbed on Si.[14] The important postulate we make is that, in cases where the reaction mechanism involves only one site in a tetrahedral environment, a single silicon atom, terminated with hydrogen, is adequate as a model for the surface.

In this paper we report ab initio molecular orbital calculations to determine the activation energies and mechanisms of reactions 3 and 4. By analogy, we estimate activation energies for reactions 1, 2, and 5. All five reactions involve either making or breaking a SiSi bond. We also have calculated the barrier to hydrogen abstraction, reaction 6, which competes with the other reactions.

$$H_3Si\text{–}SiH_3 + H^\bullet \rightarrow H_2 + [H_3Si\text{–}SiH_2]^\bullet \qquad (6)$$

As a surface reaction in plasma CVD conditions, this reaction is less interesting than the others, since it does not add or remove Si atoms from the surface, and the observable product is H_2, which is ubiquitous in the reactor. Nevertheless, the rate of this reaction has been measured in the gas phase and on the surface, and it provides another useful test of our method. Overall, comparison to experimental data shows that our simple model of the surface can provide estimates of reaction barriers that are consistent with experiments.

The Computational Model

To fully understand reaction 3, quantum mechanical methods were used to map out the minimum energy path leading from reactants to products, as illustrated in Scheme I. Following the path in the reverse direction applies to the process in reaction 4. A transition state, $[TS]^{\bullet\ddagger}$, occurs at the maximum on this reaction path. Activation energies for the forward reaction and for the reverse reaction are denoted as $E_{a,f}$ and $E_{a,r}$, respectively. The calculations (vide infra) show that there are two transition-state structures for this reaction: (1) a backside attack of the silyl group where the H atom interacts with the silicon center along the SiSi axis, forming a transition-state structure with C_{3v} symmetry, or (2) a frontside attack on the SiSi bond by the H atom (see Scheme II).

Our computational model may appear to restrict the relevance of this work to Eley–Rideal mechanisms for reaction 1. However, in interpreting experimental measurements of etching, Olander[2] has postulated that a weakly bound, mobile hydrogen is the reactive

Scheme II

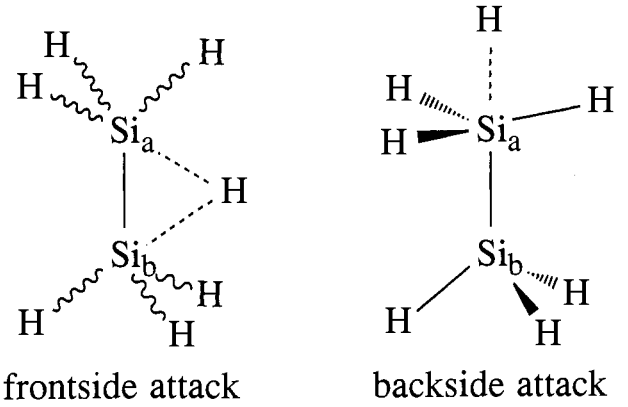

radical. Gates et al.[1] also find that hydrogen migration is facile under their etching conditions. Weakly bound hydrogen atoms on Si surfaces have been invoked to rationalize other experiments as well. Sakurai and Hagstrum[15] found evidence for such species in LEED patterns; Sinniah et al. proposed a "delocalized" H species to explain recombinative desorption of hydrogen.[16] Reactions of a weakly bound species would not require breaking a bond between hydrogen and the surface. The free hydrogen radical in our calculations may be thought of as an approximation to this weakly bound hydrogen.

The major computational goals of this work are to determine the possible transition-state structures and the relative energetics for Scheme I. Since these species have unpaired electrons, electron correlation plays an important role in both the structure determination and in the relative energetics[17] as shown by our results. There are, of course, competitive reactions to that illustrated in Scheme I (e.g., hydrogen abstraction; vide infra), but the focus of our investigation is on those simple reactions which involve the breaking (making) of the SiSi bond.

Computational Methods

All molecular orbital calculations were carried out with the Gaussian 92/90 suite of programs.[18] Metric parameters for both minima and transition-state structures were initially obtained at the Hartree–Fock (HF) level (restricted HF, RHF, for closed-shell species and unrestricted HF, UHF, for open-shell species) with the split-valence 6-31G(d,p) basis sets[19] which includes a single polarization function for Si (a d-type function) and for H (a p-type function). These same basis sets were used in the further refinement of the molecular structures by performing gradient geometry optimizations with the inclusion of correlation for all electrons at the second-order Møller–Plesset (MP2) level.[20]

A harmonic vibrational frequency analysis was carried out on each HF structure, verifying it either as a minimum (no imaginary frequencies) or a transition state (one imaginary frequency). The calculated frequencies may then be used to determine zero-point energy corrections to the total energies for these molecular structures.

Each transition-state structure was verified as belonging to reactions 3 and 4 by performing an intrinsic reaction coordinate (IRC) analysis

(13) Trucks, G. W.; Raghavachari, K.; Higashi, G. S.; Chabal, Y. J. *Phys. Rev. Lett.* **1990**, *65*, 504.
(14) Tully, J. C.; Chabal, Y. J.; Raghavachari, K.; Bowman, J. M.; Lucchese, R. R. *Phys. Rev. B* **1985**, *31*, 1184.
(15) Sakurai, T.; Hagstrum, H. D. *J. Vac. Sci. Technol.* **1976**, *13*, 807.
(16) Sinniah, K.; Sherman, M. G.; Lewis, L. B.; Weinberg, W. H.; Yates, J. T., Jr.; Janda, K. C. *Phys. Rev. Lett.* **1989**, *62*, 567; *J. Chem. Phys.* **1990**, *92*, 5700.
(17) For an example, see: Gonzalez, C.; Theisen, J.; Schlegel, H. B.; Hase, W. L.; Kaiser, E. W. *J. Phys. Chem.* **1992**, *96*, 1767.
(18) (a) Frisch, M. J.; Trucks, G. W.; Head-Gordon, M.; Gill, P. M. W.; Wong, M. W.; Foresman, J. B.; Johnson, B. G.; Schlegel, H. B.; Robb, M. A.; Replogle, E. S.; Gomperts, R.; Andres, J. L.; Raghavachari, K.; Binkley, J. S.; Gonzalez, C.; Martin, R. L.; Fox, D. J.; Defrees, D. J.; Baker, J.; Stewart, J. J. P.; Pople, J. A. *Gaussian 92*; Gaussian, Inc.: Pittsburgh, PA, 1992. (b) Frisch, M. J.; Head-Gordon, M.; Trucks, G. W.; Foresman, J. B.; Schlegel, H. B.; Raghavachari, K.; Robb, M. A.; Binkley, J. S.; Gonzalez, C.; Defrees, D. J.; Fox, D. J.; Whiteside, R. A.; Seeger, R.; Melius, C. F.; Baker, J.; Martin, R. L.; Kahn, L. R.; Stewart, J. J. P.; Topiol, S.; Pople, J. A. *Gaussian 90*; Gaussian, Inc.: Pittsburgh, PA, 1990.
(19) Francl, M. M.; Pietro, W. J.; Hehre, W. J.; Binkley, J. S.; Gordon, M. S.; DeFrees, D. J.; Pople, J. A. *J. Chem. Phys.* **1982**, *77*, 3654.
(20) Møller, C.; Plesset, M. S. *Phys. Rev.* **1934**, *46*, 618.

Table I. Total Energies (hartrees)

method	H•	H_3SiSiH_3	TS_{bs}-$[Si_2H_7]^{•‡}$	TS_{fs}-$[Si_2H_7]^{•‡}$	H_3SI•	SiH_4
HF/6-31G(d,p)//HF/6-31G(d,p)	−0.49823	−581.313 57	−581.776 96	−581.782 90	−290.610 58	−291.230 84
MP2/6-31G(d,p)//MP2/6-31G(d,p)		−581.534 62	−582.010 26	−582.015 08	−290.708 70	−291.349 86
MP2/6-311G(d,p)//MP2/6-31G(d,p)	−0.49981	−581.572 39	−582.051 40	−582.058 26	−290.727 99	−291.371 92
MP4/6-311G(d,p)//MP2/6-31G(d,p)		−581.623 69	−582.106 19	−582.113 42	−290.752 85	−291.401 36
PMP2/6-311G(d,p)//MP2/6-31G(d,p)			−582.054 77	−582.060 92	−290.728 55	
PMP4/6-311G(d,p)//MP2/6-31G(d,p)			−582.108 27	−582.114 93	−290.753 17	
QCISD(T)/6-311G(d,p)//MP2/6-31G(d,p)		−581.626 95	−582.111 87	−582.118 04	−290.754 82	−291.403 27
MP2/6-311+G(d,p)//MP2/6-31G(d,p)		−581.573 06	−582.052 16	−582.058 97	−290.728 38	−291.372 12
MP4/6-311+G(d,p)//MP2/6-31G(d,p)		−581.624 50	−582.107 09	−582.114 27	−290.753 29	−291.401 61
PMP2/6-311+G(d,p)//MP2/6-31G(d,p)			−582.055 53	−582.061 64	−290.728 93	
PMP4/6-311+G(d,p)//MP2/6-31G(d,p)			−582.109 18	−582.115 79	−290.753 61	
MP2/6-311G(2df,p)//MP2/6-31G(d,p)		−581.610 60	−582.093 28	−582.100 29	−290.744 27	−291.389 02
MP4/6-311G(2df,p)//MP2/6-31G(d,p)		−581.668 85	−582.155 32	−582.162 59	−290.772 50	−291.421 90
PMP2/6-311G(2df,p)//MP2/6-31G(d,p)			−582.096 70	−582.103 47	−290.744 89	
PMP4/6-311G(2df,p)//MP2/6-31G(d,p)			−582.157 41	−582.164 40	−290.772 85	
MP2/6-311+G(3df,2p)//MP2/6-31G(d,p)		−581.618 37	−582.102 21	−582.109 14	−290.748 41	−291.394 04
MP4/6-311+G(3df,2p)//MP2/6-31G(d,p)		−581.675 76	−582.163 66	−582.170 72	−290.776 28	−291.426 37
PMP2/6-311+G(3df,2p)//MP2/6-31G(d,p)			−582.105 63	−582.112 30	−290.749 03	
PMP4/6-311+G(3df,2p)//MP2/6-31G(d,p)			−582.165 76	−582.172 52	−290.776 63	
G1	−0.50000	−581.669 11	−582.156 96	−582.161 36	−290.773 24	−291.418 90
G2	−0.50000	−581.668 23	−582.157 15	−582.161 52	−290.773 57	−291.419 16

Table II. Equilibrium Geometries for Minima[a]

molecule	point group	metric parameter	HF/6-31G(d,p)// HF/6-31G(d,p)	MP2/6-31G(d,p)// MP2/6-31G(d,p)	expt[b]
H_3Si•	C_{3v}	r(SiH)	1.476	1.473	
		∠(HSiH)	111.0	111.2	
SiH_4	T_d	r(SiH)	1.476	1.472	1.481
Si_2H_6	D_{3d}	r(SiSi)	2.353	2.334	2.327
		r(SiH)	1.479	1.476	1.486
		∠(HSiSi)	110.4	110.3	111.0

[a] Bond lengths in Å and bond angles in degrees. [b] Callomon, J. H.; Hirota, E.; Kuchitsu, K.; Lafferty, W. J.; Maki, A. G.; Pote, C. S. *Structure Data on Free Polyatomic Molecules* (Landolt-Bornstein, New Series, Group II, Vol. 7); Springer-Verlag: Berlin, 1976.

at the HF level.[21] This analysis examines the steepest-decent reaction path leading down from the transition state to both the reactants and the products. The molecular geometry is optimized at each point along the reaction path.

To determine reliable relative energetic data, we carried out a series of single-point energy calculations on the MP2/6-31G(d,p) geometries with successively larger basis sets and with different electron correlation methods. These data are summarized in Table I. The largest basis sets in these energy calculations, 6-311+G(3df,2p),[22,23] include diffuse functions on silicon as well as three d-type and one f-type polarization functions on silicon and two p-type polarization functions on hydrogen. MP2 and MP4 refer to the Møller–Plesset electron correlation methods in which the latter method includes single, double, triple, and quadruple ("SDTQ") excitations. Since the energies of the open-shell species were calculated by unrestricted MP*n* methods, an approximate spin projection method[24] was used to remove contamination from higher spin states (denoted by PMP*n* in Tables I and III). QCISD(T) is a quadratic configuration interaction scheme with all single and double substitutions and a partial treatment of triple substitutions.[25] Relative energies were also calculated within Gaussian 1 (G1) and Gaussian 2 (G2) theories.[26-28] These methods are empirically derived computational procedures for predicting total energies which are useful for calculating atomization energies, ionization energies, proton affinities, and electron affinities to within 3 kcal mol^{-1} of experiment. The G2 theoretical procedure eliminates some deficiencies in the G1 theory. Table IV contains the relevant data needed (along with data from Table III) to generate the G1 and G2 energies. We adhered to the G1 and G2 methodologies with one exception: the molecular geometries used in this work were calculated using the 6-31G(d,p) basis sets instead of the recommended 6-31G(d) basis sets. Finally, all reported single-point energy calculations correlated only the valence electrons.

Results

Molecular Geometries. The computed equilibrium geometries for the ground-state molecules are tabulated in Table II along with the available experimental values. The geometries optimized with electron correlation at the MP2 level and with the 6-31G(d,p) basis sets are in good agreement with experiment (the bond lengths and bond angles agree to within 0.01 Å and 1°, respectively). Note that the best calculated value for the SiSi bond length (2.334 Å) is slightly shorter than the interatomic distance (2.352 Å) in bulk silicon.

We now turn to the MP2 geometries of the transition-state structures for reactions 3 and 4 as shown in Figures 1 and 2. The numbers in square brackets are the respective HF metric parameters. In both figures, one may imagine the top silicon moiety representing the trihydride species of silicon (Si_a) on the surface and the bottom silicon atom representing a bulk silicon atom (Si_b). As expected, the incoming H atom affects the local geometry of Si_a more than the other silicon.

The importance of electron correlation in calculating open-shell transition-state structures is evident in the frontside attack of disilane by a hydrogen atom, TS_{fs}. In the HF geometry, the TS_{fs} structure shows the incoming H atom as more closely associated with Si_a and affecting its geometry more than that around Si_b. This results in a strong five-coordinate environment around Si_a while Si_b remains primarily four-coordinate. Also, note that the HF SiSi bond length is significantly longer (~0.13 Å) than that found in disilane. However, the MP2 metric parameters show a different structure in which the attacking hydrogen bridges the two silicons in a near-symmetric manner.

(21) Gonzalez, C.; Schlegel, H. B. *J. Chem. Phys.* **1989**, *90*, 2154.
(22) Clark, T.; Chandrasekhar, J.; Spitznagel, G. W.; Schleyer, P. v. R. *J. Comput. Chem.* **1983**, *4*, 294.
(23) Frisch, M. J.; Pople, J. A.; Binkley, J. S. *J. Chem. Phys.* **1984**, *80*, 3265.
(24) Schlegel, H. B. *J. Chem. Phys.* **1986**, *84*, 4530.
(25) Pople, J. A.; Head-Gordon, M.; Raghavachari, K. *J. Chem. Phys.* **1984**, *87*, 5968.
(26) Pople, J. A.; Head-Gordon, M.; Fox, D. J.; Raghavachari, K.; Curtiss, L. A. *J. Chem. Phys.* **1989**, *90*, 5622.
(27) Curtiss, L. A.; Jones, C.; Trucks, G. W.; Raghavachari, K.; Pople, J. A. *J. Chem. Phys.* **1990**, *93*, 2537.
(28) Curtiss, L. A.; Raghavachari, K.; Trucks, G. W.; Pople, J. A. *J. Chem. Phys.* **1991**, *94*, 7221.

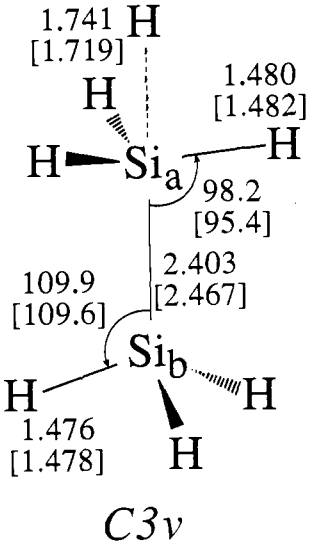

Figure 1. MP2/6-31G(d,p) metric parameters for the backside transition-state structure, TS_{bs}, in reaction 3. HF/6-31G(d,p) metric parameters are given in parentheses for comparison. Bond lengths and bond angles are given in Å and degrees, respectively.

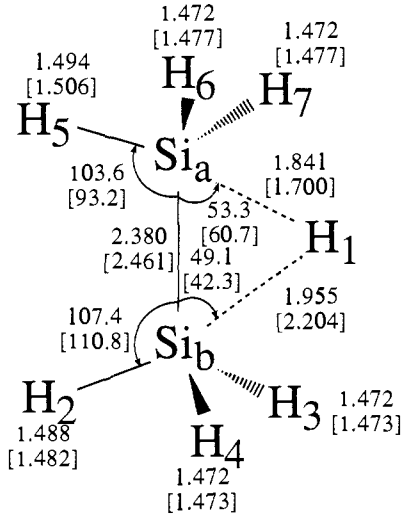

$\angle(H_3Si_bSi_a) = \angle(H_4Si_bSi_a) = 111.2\ [108.2]$
$\angle(H_6Si_aSi_b) = \angle(H_7Si_aSi_b) = 113.7\ [118.9]$
$\omega(H_2Si_bSi_aH_1) = \omega(H_5Si_aSi_bH_1) = 180.0\ [180.0]$
$\omega(H_3Si_bSi_aH_2) = -\omega(H_4Si_bSi_aH_2) = 117.4\ [120.0]$
$\omega(H_6Si_aSi_bH_5) = -\omega(H_7Si_aSi_bH_5) = 114.6\ [107.3]$

Figure 2. MP2/6-31G(d,p) metric parameters for the frontside transition-state structure, TS_{fs}, in reaction 3. HF/6-31G(d,p) metric parameters are given in parentheses for comparison. Bond lengths and bond angles are given in Å and degrees, respectively.

The bridging hydrogen is still closer to Si_a (1.898 Å) than to Si_b (1.932 Å), but the difference in these SiH distances is smaller (~0.03 Å) than the corresponding HF value (~0.50 Å). The MP2 SiSi bond is not nearly as elongated as the HF SiSi bond, and it has a length (2.377 Å) which is about 0.04 Å longer than the corresponding value in disilane. Both silicon centers in the MP2 structure are five-coordinate and have nearly identical structural environments for the nonbridging hydrogens. Note that the two hydrogens which are trans to the bridging hydrogen have longer bond lengths to their respective silicons than the other four hydrogens. These trans hydrogens may be thought of as "axial" hydrogens in trigonal bipyramidal silicon while the remaining hydrogen atoms are in the "equatorial" positions. The difference in axial and equatorial bond distances is similar to that

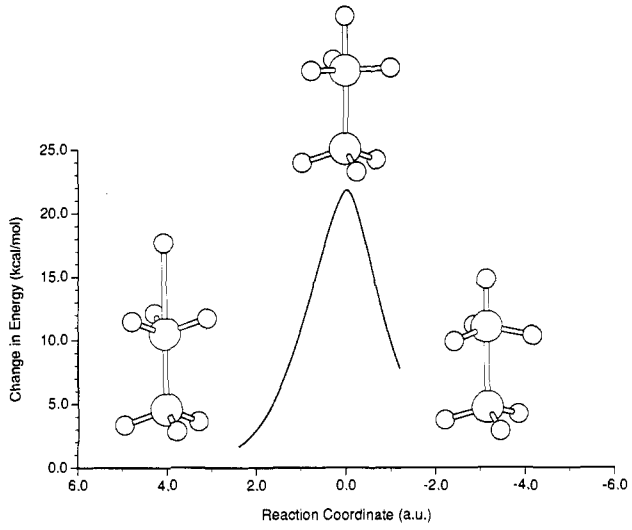

Figure 3. Minimum energy pathway at the HF/6-31G(d,p) level near the transition state for backside attack (au is equivalent to $amu^{1/2}$ bohr). The structures correspond to the maximum and the endpoints of the drawn curve. The left structure is the initial interaction of H• with Si_2H_6, the middle structure is the backside transition-state structure, and the right structure is the separation of SiH_4 from H_3Si•.

found in the transition-state structure, $[SiH_5]^{\bullet\ddagger}$, for the reaction of H• with SiH_4.[29]

The calculated transition-state structure for backside attack, TS_{bs}, is also affected by inclusion of electron correlation. The overall HF structure has a strong five-coordinate environment around Si_a and a near-tetrahedral geometry around Si_b. Tachibana et al. have recently reported a HF structure for this same transition state.[30] Since the 6-31G* basis sets were used (no polarization functions for hydrogen) in this calculation, there is a negligible difference between the two HF structures. This qualitative description also applies to the MP2 structure of the current work. The equatorial SiH bonds for Si_a almost all lie in a plane, lacking 8° from an ideal trigonal bipyramidal structure, and the corresponding bond lengths are nearly identical with those in $[SiH_5]^{\bullet\ddagger}$.[29] The metric parameters for the local environment around Si_b have not significantly changed from corresponding values in disilane. The two main differences between the MP2 and the HF structures are the longer SiH bond distance for the incoming hydrogen and the shorter SiSi bond distance for the MP2 structure compared to the HF structure. It is interesting to note that this MP2 SiH bond length lies halfway between the relatively short axial bond length for $[SiH_5]^{\bullet\ddagger}$[29] and the relatively long SiH bond length for the bridging hydrogen in TS_{fs}. The MP2 SiSi bond length is almost 0.03 Å longer than the corresponding value in TS_{fs}.

Relative Energetics. The minimum energy paths (at the HF level) for backside and frontside attack of disilane by a hydrogen atom are illustrated in Figures 3 and 4, respectively. These two figures clearly show that the two calculated transition-state structures are possible for reaction 3. Early in the backside attack, the SiH bonds are already bending away from the approaching hydrogen atom. Both this umbrella motion of the SiH bonds and the elongation of the SiSi bond continue through the transition state on toward products. The minimum energy path for frontside attack is not as symmetric as the one for the backside attack because of the more complicated motion of the affected atoms in the frontside attack. In approaching the transition state, the major motion is the rocking of the "top-most" SiH_3 moeity away from the in-coming hydrogen atom. Beyond the transition state, this same rocking motion continues, causing the "bottom-most"

(29) Dobbs, K. D. Unpublished calculations.
(30) Tachibana, A.; Kurosaki, J.; Yamaguchi, K.; Yamabe, T. *J. Phys. Chem.* **1991**, *95*, 6849.

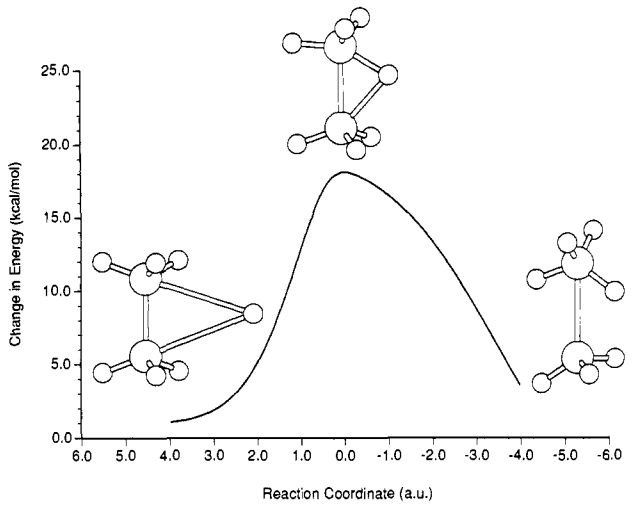

Figure 4. Minimum energy pathway at the HF/6-31G(d,p) level near the transition state for frontside attack (au is equivalent to amu$^{1/2}$ bohr). The structures correspond to the maximum and the endpoints of the drawn curve. The left structure is the initial interaction of H$^{\bullet}$ with Si_2H_6, the middle structure is the frontside transition-state structure, and the right structure is the separation of SiH_4 from $H_2Si^{\bullet}$.

SiH_3 moeity to rock in the same direction and, thereby, lessen the steric interaction between the eclipsing hydrogens of these two SiH_3 moeities.

Table III contains the forward and reverse enthalpies of activation for the frontside and backside attacks, as well as the overall enthalpy of reaction, at all levels of theory considered in this work for the reaction illustrated in Scheme I. All numbers have been corrected for zero-point energy. Both G2 theory and the PMP4/6-311+G(3df,2p)//MP2/6-31G(d,p) level give nearly the same numbers for the forward and reverse activation enthalpies for both the backside attack ($\sim$7 and $\sim$22 kcal mol^{-1}, respectively) and the frontside attack ($\sim$4 and $\sim$19 kcal mol^{-1}, respectively) of disilane by a hydrogen atom. Tachibana et al. performed similar calculations for this same reaction but only investigated the transition state for backside attack.[30] Their best numbers for the forward and reverse activation enthalpies are $\sim$11 and $\sim$30 kcal mol^{-1}, respectively. These higher numbers are the result of using geometries optimized without the inclusion of electron correlation and performing single-point correlated calculations with a smaller basis set than in the current work. Our calculations show that the forward reaction encounters a rather low energy barrier, with the transition state for the frontside attack being about 3 kcal mol^{-1} lower in energy than for the backside attack. Also, note from Table III that this relative difference of about 3 kcal mol^{-1} between the two energy barriers was maintained for all methods of calculation.

To compare the 0 K data in Table III to experimental enthalpies at room temperature, we need to include the contributions of translational, rotational, and vibrational energies[31] between 0 K and 298 K. These energy corrections can be easily evaluated, given the calculated structure and vibrational frequencies. The corrected energy values have been tabulated only for the PMP4/6-311+G(3df,2p)//MP2/6-31G(d,p), G1, and G2 methods in Table V along with their uncorrected values. Note that these corrections lowered the activation enthalpies, $\Delta H^{\ddagger\circ}$, by no more than 1.3 kcal mol^{-1} and left the overall enthalpy, ΔH, of reaction essentially unchanged. The Arrhenius activation energy, E_a, is related to $\Delta H^{\ddagger\circ}$ by,[32]

$$E_a = \Delta H^{\ddagger\circ} + RT \quad (7)$$

Activation energies determined from the corrected activation enthalpies are also tabulated in Table V. From now on, any mention of energetic data from our work will refer to the results at the PMP4/6-311+G(3df,2p)//MP2/6-31G(d,p) level since this level of theory is straightforward and does not involve a composite theoretical procedure.

The idealized reaction path profile in Figure 5 summarizes the relative energetics of the gas-phase reaction for a hydrogen atom breaking the SiSi bond in disilane. The forward reaction is exothermic, and the activation energy for either transition state is relatively small. These results alone point to a facile reaction for cleaving SiSi bonds with hydrogen atoms. However, this exchange reaction has a strong competing reaction, namely, hydrogen abstraction, reaction 6. The activation barrier, E_a, for H abstraction at the PMP4/6-311+G(3df,2p)//MP2/6-31G(d,p) level (structures and energies are given in Tables VI and VII, respectively) is 3.4 kcal mol^{-1} which is slightly higher than the barrier for frontside attack (3.2 kcal mol^{-1}).

For hydrogen radical reactions, tunneling corrections may be significant. We have estimated these corrections with the Wigner approximations.[33] This approximation introduces a temperature-dependent transmission factor,

$$\kappa = 1 + \frac{1}{24}\left|\frac{h\nu^{\ddagger}}{k_B T}\right|^2 \quad (8)$$

where h is Planck's constant, $\nu^{\ddagger}$ is the imaginary frequency at the transition state, k_B is Boltzmann's constant, and T is the temperature. This factor is significantly greater than one when the barrier is narrow (i.e., when the imaginary frequency at the transition state is large) and introduces curvature into the Arrhenius plot, so that the apparent activation energy is temperature dependent. The transition states for frontside attack, backside attack, and abstraction have imaginary frequencies of 460 cm^{-1}, 1350 cm^{-1}, and 2025 cm^{-1}, respectively. At 298 K, these lead respectively to corrections to the activation energies of -0.2 kcal mol^{-1}, -0.8 kcal mol^{-1}, and -1.0 kcal mol^{-1}. Therefore, the tunneling-corrected activation energies are 3.0 kcal mol^{-1} for frontside attack, 5.8 kcal mol^{-1} for backside attack, and 2.4 kcal mol^{-1} for abstraction. Note that, after tunneling corrections are included, the barrier for hydrogen abstraction is 0.6 kcal mol^{-1} lower than that for frontside attack, while, without tunneling, the frontside attack is energetically favored. Thus, tunneling effects are essential for understanding the relative rates of these reactions. For accurate predictions of reaction rates, the Wigner approximation may be too crude.

Discussion

Our model calculations provide a reliable description of gas-phase reactions of hydrogen radicals with disilane. We can make several direct comparisons with experiments. Fabry et al.[11] have measured the combined rate of exchange (reaction 3) and hydrogen abstraction (reaction 6). The activation energy for the pseudo-first-order rate of hydrogen radical disappearance is 2.3 $\pm$ 0.2 kcal mol^{-1}, which is in very good agreement with the 2.4-kcal mol^{-1} barrier that we have predicted for abstraction. From isotopic substitution Fabry et al.[11] estimated that the abstraction reaction is three to four times faster than exchange. Pollock et al.[34] found that abstraction was twice as fast as exchange. Assuming that the Arrhenius prefactors for these two reactions are the same, this difference in rates implies that the barrier to abstraction is 0.4–0.8 kcal mol^{-1} lower than the barrier to exchange. Our calculations concur, indicating a difference of 0.6 kcal mol^{-1} between these two reaction barriers. To determine

(31) Hehre, W. J.; Radom, L.; Schleyer, P. v. R.; Pople, J. A. *Ab Initio Molecular Orbital Theory*; Wiley: New York, 1986; pp 258–260.

(32) This equation is derived from the relationship between Arrhenius' activation theory and Eyring's transition-state theory. See any undergraduate physical chemistry book, for example: Daniels, F.; Alberty, R. A. *Physical Chemistry*, 4th ed.; Wiley: New York, 1975; pp 318–322.

(33) Wigner, E. P. *Z. Phys. Chem.* **1932**, *B19*, 203.

(34) Pollock, T. L.; Sandhu, H. S.; Jodhan, A.; Strausz, O. P. *J. Am. Chem. Soc.* **1973**, *95*, 1017.

Table III. Relative Energetics (kcal mol^{-1})[a]

method	$\Delta H_f^{*\circ}$(0 K)		$\Delta H_r^{*\circ}$(0 K)		
	TS_{bs}	TS_{fs}	TS_{bs}	TS_{fs}	ΔH(0 K)
HF/6-31G(d,p)//HF/6-31G(d,p)	22.7	20.1	39.3	36.6	-16.6
MP2/6-31G(d,p)//MP2/6-31G(d,p)	15.0	13.1	29.1	27.2	-14.1
MP2/6-311G(d,p)//MP2/6-31G(d,p)	13.9	10.7	29.3	26.1	-15.4
MP4/6-311G(d.p)//MP2/6-31G(d,p)	11.7	8.3	28.9	25.5	-17.3
PMP2/6-311G(d,p)//MP2/6-31G(d,p)	11.8	9.0	27.5	24.7	-15.7
PMP4/6-311G(d.p)//MP2/6-31G(d,p)	10.4	7.3	27.8	24.8	-17.5
QCISD(T)/6-311G(d,p)//MP2/6-31G(d,p)	10.2	7.4	27.8	25.1	-17.6
MP2/6-311+G(d,p)//MP2/6-31G(d.p)	13.8	10.7	29.1	26.0	-15.3
MP4/6-311+G(d,p)//MP2/6-31G(d.p)	11.6	8.2	28.8	25.4	-17.2
PMP2/6-311+G(d,p)//MP2/6-31G(d,p)	11.7	9.0	27.4	24.6	-15.7
PMP4/6-311+G(d,p)//MP2/6-31G(d,p)	10.3	7.3	27.7	24.7	-17.4
MP2/6-311G(2df,p)//MP2/6-31G(d.p)	11.6	8.3	23.9	20.6	-12.3
MP4/6-311G(2df,p)//MP2/6-31G(d,p)	9.2	5.7	23.3	19.9	-14.1
PMP2/6-311G(2df.p)//MP2/6-31G(d,p)	9.4	6.3	22.2	19.0	-12.7
PMP4/6-311G(2df,p)//MP2/6-31G(d.p)	7.9	4.6	22.2	19.0	-14.4
MP2/6-311+G(3df,2p)//MP2/6-31G(d,p)	10.9	7.6	24.1	20.8	-13.2
MP4/6-311+G(3df,2p)//MP2/6-31G(d,p)	8.3	5.0	23.3	20.0	-15.0
PMP2/6-311+G(3df.2p)//MP2/6-31G(d.p)	8.7	5.6	22.3	19.2	-13.6
PMP4/6-311+G(3df,2p)//MP2/6-31G(d,p)	7.0	3.8	22.2	19.0	-15.2
G1	7.6	4.9	22.1	19.3	-14.5
G2	7.0	4.2	22.3	19.6	-15.4

[a] $\Delta H_f^{*\circ}$ and $\Delta H_r^{*\circ}$ refer to the forward and reverse activation enthalpies, respectively, for reaction 3. ΔH is the overall enthalpy for reaction 3.

Table IV. Relevant Energy Corrections for Reproducing G1 and G2 Energies (millihartrees)

corrections	H$^\bullet$	H_3SiSiH_3	TS_{bs}	TS_{fs}	$H_3Si^\bullet$	SiH_4
ΔE(HLC)	-0.19	-42.98	-43.17	-43.17	-18.61	-24.56
ΔE(ZPE)		46.79	48.11	49.87	20.28	29.72
Δ		-7.10	-8.17	-8.14	-3.75	-4.82
1.14*n*pair		7.98	7.98	7.98	3.42	4.56

the mechanism of the exchange reaction, Fabry et al.[11] also studied reactions of hydrogen radicals with substituted disilanes. They inferred that the exchange reaction occurs by a frontside attack, and our results provide further support for their conclusion. The gas-phase reactions of silyl radicals with silane (reaction 4) is endothermic and is expected to be slow at room temperature. Loh and Jasinski[12] have measured the rate of this reaction directly and find that it is so slow that they can only determine an upper bound to the rate.

Our results can also be compared to experimental observations for surface reaction rates. We first consider etching, reaction 1. Both infrared spectroscopy[35,36] and static SIMS measurements[7,37] show the presence of surface SiH_3 on hydrogen saturated Si(111) and Si(100) surfaces. Cheng and Yates[38] have observed SiH_4 produced in thermal desorption experiments on H-covered Si(100) in the (1 × 1) phase but not in the (3 × 1) phase. They interpret this as evidence for the presence of SiH_3 on the (1 × 1) surface. This interpretation is supported by electronic structure calculations by Vittadini et al.[39] which show that formation of adsorbed SiH_3 species is thermodynamically favored on the H-saturated Si(100)–(1 × 1) surface.

The trihydride sites are typically present at densities of a few percent of a monolayer. If the reactive hydrogenic species can be approximated as a hydrogen radical, our calculation should provide a good estimate of the barrier to etching the trihydride species. Abrefah and Olander[2] observed etching kinetics on Si(111) under conditions with a high flux of atomic H. Their model assumes that all dangling bonds are saturated and that the predominant surface species is the dihydride. The rate-limiting step is production of the trihydride from the dihydride. Etching of the trihydride is assumed to be fast. They derive an activation barrier of about 2 kcal mol^{-1} for the overall two-step process. This is necessarily an upper bound to the barrier for reaction 1, but given the experimental uncertainties and model dependence of the value, it is remarkably close to our prediction of 3.0 kcal mol^{-1}. Gates et al.[1] studied etching from a hydrogen-covered (100) surface using temperature-programmed desorption. Adsorbed hydrogen was present, but no additional hydrogen was incident from the gas phase during heating. They find that the rate of silane production is proportional to the density of surface trihydride as measured by SIMS. They do not derive an activation barrier for this reaction, but it is clearly activated. Etching increases with temperature up to 375 °C, at which point decomposition of the surface trihydride becomes important. A small activation barrier, comparable to that in our model, is consistent with their observations.

We now turn to the deposition process, reaction 2, which is the reverse of etching. Silicon surface growth from silane adsorption has been the subject of many experiments over the last 2 decades. There have been excellent reviews in recent years,[9,40,41] and a kinetic model has been developed that describes Si film growth from low-pressure SiH_4 over a wide range of surface temperature and hydrogen coverage.[8] This previous work has shown that, on Si surfaces with a high coverage of dangling bonds, the surface deposition process is limited by the initial silane adsorption step. Estimates of the activation barrier for this step are ≲5 kcal mol^{-1}. However, under steady-state growth conditions, surface dangling bonds are saturated with hydrogen at temperatures below about 600 °C. On surfaces with few dangling bonds, the rate is determined by the availability of open sites. Thus, hydrogen desorption, with an activation barrier of over 40 kcal mol^{-1},[16,42] is the rate-limiting step at low temperatures. Gates et al.[7,8] have postulated that on the clean Si(100)–(2 × 1) surface, silane adsorption takes place only if two adjacent dangling bonds are available; an SiH bond in silane is broken to form SiH_3 and H radicals which adsorb at the two sites. If the transition state of this reaction involves both dangling bond sites, our model can only provide an upper bound to the activation barrier for adsorption. Comparing the 0–5 kcal mol^{-1} experimental activation

(35) Chabal, Y. J.; Higashi, G. S.; Raghavachari, K.; Burrows, V. A. *J. Vac. Sci. Technol. A* **1989**, *7*, 2104.
(36) Jansson, U.; Uram, K. J. *J. Chem. Phys.* **1989**, *91*, 7978.
(37) Greenlief, C. M.; Gates, S. M.; Holbert, P. A. *Chem. Phys. Lett.* **1989**, *159*, 202.
(38) Cheng, C. C.; Yates, J. T., Jr. *Phys. Rev. B* **1991**, *43*, 4041.
(39) Vittadini, A.; Seloni, A.; Car, R.; Casarin, M. *Phys. Rev. B* **1992**, *46*, 4348.
(40) Buss, R. J.; Ho, P.; Breiland, W. G.; Coltrin, M. E. *J. Appl. Phys.* **1988**, *63*, 2808.
(41) Comfort, J. H.; Reif, R. *J. Electrochem. Soc.* **1989**, *136*, 2386.
(42) Koehler, B. G.; Mak, C. H.; Arther, D. A.; Coon, P. A.; George, S. M. *J. Chem. Phys.* **1988**, *89*, 1709.

Table V. Comparison of Uncorrected and Corrected Enthalpies, ΔH, with Activation Energies, E_a (kcal mol^{-1}) for Reaction 3

method	activation parameter	temp (K)	forward reaction TS_{bs}	forward reaction TS_{fs}	reverse reaction TS_{bs}	reverse reaction TS_{fs}
PMP4/6-311+G(3df,2p)//MP2/6-31G(d,p)	$\Delta H^{\ddagger\circ}$	0	7.0	3.8	22.2	19.0
	$\Delta H^{\ddagger\circ}$	298	6.0	2.6	21.3	17.9
	E_a	298	6.6	3.2	21.9	18.5
G1	$\Delta H^{\ddagger\circ}$	0	7.6	4.9	22.1	19.3
	$\Delta H^{\ddagger\circ}$	298	6.6	3.6	21.2	18.2
	E_a	298	7.2	4.2	21.8	18.8
G2	$\Delta H^{\ddagger\circ}$	0	7.0	4.2	22.3	19.6
	$\Delta H^{\ddagger\circ}$	298	6.0	2.9	21.5	18.5
	E_a	298	6.6	3.5	22.1	19.1

method	temp (K)	ΔH
PMP4/6-311+G(3df,2p)//MP2/6-31G(d,p)	0	−15.2
	298	−15.3
G1	0	−14.5
	298	−14.6
G2	0	−15.4
	298	−15.5

Summary of Relative Energetics

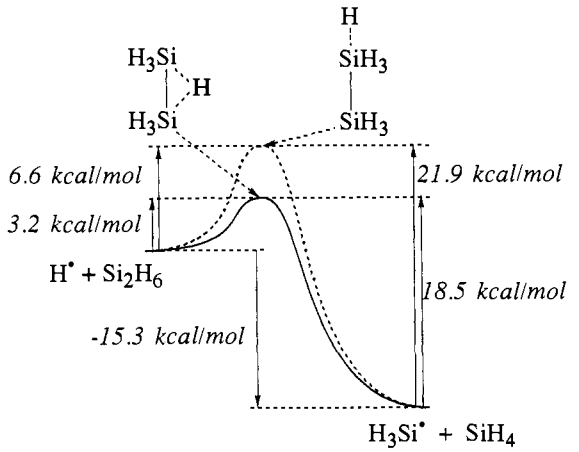

Figure 5. Idealized reaction path profile for the gas-phase reaction of a hydrogen atom cleaving the SiSi bond in disilane. The relative energetics do not include corrections for tunneling.

barrier to the 18.5 kcal mol^{-1} activation energy in our model indicates that the transition state for silane adsorption must be stabilized by an empty adjacent site. In contrast, on H-covered surfaces, where the probability is low for two adjacent sites to be empty, our model suggests that adsorption with loss of a hydrogen radical (that does not go on to fill a dangling bond) may compete with other high activation barrier processes. On the Si(111)–(7 × 7) surface, where dangling bonds are farther apart than on Si(100)–(2 × 1), Farnaam and Olander[6] and Gates et al.[7] have argued that SiH_4 loses two hydrogens in the initial adsorption step to form SiH_2 directly. If this is the case, our model reactions give no additional insight to the energetics of this process since the transition state studied does not lead to the correct products. However, the large barrier we find to formation of the trihydride from silane confirms that this mechanism for dissociative adsorption is unfavorable. All of the comments made about reaction 2 apply to the similar reaction 5, leading to the conclusion that reaction 5 is likely to occur only if the product H can be adsorbed or recombined with another adsorbed H to make H_2.

Finally, we turn to the heterogeneous abstraction of H_2, which is the surface analogue of reaction 6. Abrefah and Olander[2] derive an activation barrier of 4.5 kcal mol^{-1} for this reaction. Sinniah et al.[16] have made direct measurements of abstraction from a deuterium-covered surface by gas-phase hydrogen atoms. Within the accuracy of their data, the abstraction rate is independent of temperature down to 125 K. This evidence is consistent with a small activation barrier, but Sinniah et al.[16] suggest, as a more likely interpretation, that the incoming

Table VI. Equilibrium Geometries for the Hydrogen Abstraction Transition-State Structure and the Products in Reaction 7[a]

molecule	point group	metric parameter[b]	MP2/6-31G(d,p)// MP2/6-31G(d,p)
TS_{ab}–$[Si_2H_7]^{\bullet\ddagger}$	C_s	$r(Si_aSi_b)$	2.332
		$r(Si_aH_1)$	1.607
		$r(H_1H_2)$	1.100
		$r(Si_aH_3)$	1.477
		$r(Si_bH_4)$	1.476
		$r(Si_bH_5)$	1.476
		$\angle(H_1H_2Si_a)$	180.0
		$\angle(H_1Si_aSi_b)$	109.4
		$\angle(H_3Si_aSi_b)$	111.7
		$\angle(H_4Si_bSi_a)$	109.8
		$\angle(H_5Si_bSi_a)$	111.0
		$\omega(H_3Si_aSi_bH_1)$	±118.9
		$\omega(H_4Si_bSi_aH_1)$	180.0
		$\omega(H_5Si_bSi_aH_1)$	±59.8
H_2	$D_{\infty h}$	$r(HH)$	0.734
$[Si_2H_4]^{\bullet}$	C_s	$r(Si_aSi_b)$	2.325
		$r(Si_aH_1)$	1.476
		$r(Si_bH_2)$	1.477
		$r(Si_bH_3)$	1.475
		$\angle(H_1Si_aSi_b)$	114.0
		$\angle(H_2Si_bSi_a)$	112.3
		$\angle(H_3Si_bSi_a)$	109.2
		$\omega(H_1Si_aSi_bH_2)$	±63.6
		$\omega(H_3Si_bSi_aH_2)$	±120.5

[a] Bond lengths in Å and bond angles in degrees. [b] For the silicon hydride structures, the metric parameters refer to the following figures:

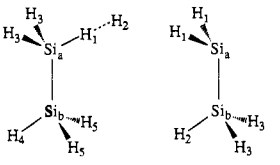

hydrogen does not accommodate to the surface temperature before reacting. They describe the abstraction as a "generalized Eley–Rideal" mechanism. The reaction is very efficient; Sinniah et al.[16] show that the probability of removing an adsorbed deuterium is of the same order as the sticking probability for hydrogen. The activation energy of 2.4 kcal mol^{-1} that we have determined for gas-phase abstraction from disilane supports the conclusion that the activation energy for abstraction is low. Detailed comparisons to surface reactions are problematic since abstraction from the surface is more likely to occur from the more common monohydride or dihydride sites than from a trihydride site like that in our model. Furthermore, in our calculations, the activation energy for abstraction is lower than that for etching, which reverses the order proposed by Abrefah and Olander.[2] However, the differ-

Table VII. Total Eneriges and Zero-Point Energies, ZPE (in hartrees), for the Hydrogen-Abstraction Transition-State Structure, TS_{ab}, and the Products in Reaction 7

method	TS_{ab}–$[Si_2H_7]^{\bullet *}$	$[H_3SiSiH_2]^{\bullet}$	H_2
MP2/6-31G(d,p)//MP2/6-31G(d,p)	-582.017 65	-580.898 10	-1.157 66
PMP4/6-311+G(3df,2p)//MP2/6-31G(d.p)	-582.168 65	-581.031 19	-1.170 19
ZPE	0.045 70	-0.037 91	0.013 95

ences among these activation barriers are small in absolute terms and are close to the limits of accuracy for both experiment and theory.

Conclusion

High-level electronic structure methods are accurate in reproducing activation energies for gas-phase radical reactions of silicon hydrides. To make accurate predictions within 1 kcal mol^{-1} for reactions containing unpaired electrons, it is essential to include electron correlation effects for molecular structure determination and for relative energetics. In this study, geometry optimizations were performed at the MP2 level with large basis sets [6-31G(d,p)] which includes polarization for all atoms. Using these optimized geometries, an additional set of calculations, which utilize very large basis sets with multiple polarization functions [6-311+G(3df,2p)], were carried out at a very high level of correlation (PMP4) to obtain the relative energetics.

Our calculations strongly support the conclusions of Fabry et al.[11] that cleaving the SiSi bond in disilane with hydrogen atoms will proceed by a frontside attack of the SiSi bond (E_a = 3.0 kcal mol^{-1}) rather than by a backside attack of the silyl group (E_a = 5.8 kcal mol^{-1}). Also, our calculations indicate that a strong competing reaction to frontside attack is hydrogen abstraction (E_a = 2.4 kcal mol^{-1}). These computational results compare very well with gas-phase experiments of hydrogen atom reactions with disilane, demonstrating the accuracy of the energetics and the mechanistic insight that can be gained from ab initio molecular orbital methods.

The similarities between activation barriers measured for these gas-phase reactions and their surface analogues suggest that a small cluster of silicon atoms is adequate to model reactions on a silicon surface. The uncertainty in current experimental measurements of surface reaction energetics is too large to expose any failures of this model. Of course, the cluster model must include enough silicon atoms to model the variety of sites that take part in the reaction. On reconstructed surfaces, where Si atoms may not have a nearly tetrahedral geometry, it remains to demonstrate that calculations on small clusters can effectively model surface reactions. The preliminary evidence provided by these calculations indicates that it is not necessary to include many other atoms simply to provide a "bath" of electronic states around the reaction site. Similar conclusions have been reached by Wu and Carter,[43] who have used cluster models to study reactions of fluorine on the reconstructed Si(100)–(2 × 1) surface.

This computational work provides essential insight into the role of competing reaction pathways. Even in the gas phase, the mechanism of reaction 3 has not been determined unambiguously by experiment. Reaction conditions on a surface can favor a mechanism different from that in the gas phase. For example, in gas-phase reaction 3, the activation barriers for frontside and backside attack differ by only 3 kcal mol^{-1}. On a hydrogen-covered surface, with no ambient gas-phase hydrogen, surface reaction 1 can only occur by a Langmuir–Hinshelwood mechanism. Thus, surface reaction conditions would favor frontside attack, even if it were not energetically favorable in the gas phase. A fundamental advantage that computational studies have over gas-phase experiments is the ability to study reaction mechanisms that are not likely in the gas phase, but may be important under surface reaction conditions.

The present work concerns only one elementary step in the etching of a silicon surface by hydrogen atoms. Our simple model does not distinguish surface reactions at different types of sites. For example, this model would predict that the energy barrier to formation of the surface trihydride (from the dihydride) is the same as the barrier to formation of silane (from the trihydride). Each of these reactions involves breaking a SiSi bond and forming a SiH bond, but they occur at different types of sites. With a model as small as the one we have used, both sites are modeled the same way. This can be a good model only if the mechanism and activation energies of these two reactions are similar. Further computational work, using an extended model with multiple sites, is needed to fully understand silicon surface etching by hydrogen.

Acknowledgment. D.J.D. acknowledges the Donors of the Petroleum Research Fund, administered by the American Chemical Society, for the partial support of this research. The work on which this material is based was also supported by the National Science Foundation under Grant No. CHE-9015368. K.D.D. thanks David Dixon for helpful suggestions in preparing the manuscript for publication.

(43) Wu, C. J.; Carter, E. A. *Phys. Rev. B* **1992**, *45*, 9065.